Laser Shocking Tuning Dynamic Interlayer Coupling In Graphene-Boron Nitride Moiré Superlattices

Prashant Kumar[1,2,6,‡], Jing Liu[3,4,7,‡], Maithilee Motlag[1‡], Lei Tong[12,‡], Yaowu Hu[1,2,8], Xinyu Huang[12], Arkamita Bandopadhyay[9,10], Swapan K. Pati[9], Lei Ye[12,*], Joseph Irudayaraj[3,4,11,*], Gary J. Cheng[1,2,5,*]

1. Department of Industrial Engineering, 2. Birck Nanotechnology Centre, 3. Bindley Bioscience Centre, 4. Department of Agriculture Biological Engineering, 5. Department of Mechanical Engineering, Purdue University, West Lafayette, IN 47907, USA.

6. Department of Physics, Indian Institute of Technology Patna, Bihta Campus, Bihta, Bihar -801106, INDIA.

7. Indiana University-Purdue University Indianapolis, Indianapolis, IN 46202, USA

8. University at Buffalo—SUNY, 3435 Main Street, Buffalo, NY 14214, USA

9. Theoretical Sciences Unit, Jawaharlal Nehru Centre for Advanced Scientific Research, Bangalore-560064, INDIA,

10. University of Pennsylvania, Philadelphia, PA 19104, USA.

11. University of Illinois at Urbana-Champaign, 1304 W. Springfield Ave. Urbana, IL 61801, USA.

12. School of Optical and Electronic Information， Huazhong University of Science and Technology, Luoyu Road 1037, Wuhan, 430074, China

‡,* These authors have equal contributions.

This is the author's manuscript of the article published in final edited form as:

Kumar, P., Liu, J., Motlag, M., Tong, L., Hu, Y., Huang, X., … Cheng, G. J. (2018). Laser shocking tuning dynamic interlayer coupling in graphene-boron nitride moiré superlattices. Nano Letters. https://doi.org/10.1021/acs.nanolett.8b03895

Abstract:

Following in the emerging of graphene and many two-dimensional (2D) materials, the most exciting applications come from stacking them into 3D devices, promising many excellent possibilities for neoteric electronics and optoelectronics. Layers of semiconductors, insulators and conductors can be stacked to form van der Waals heterostructures, after the weak bonds formed between the layers. However, the interlayer coupling in these heterostructures is usually hard to modulate, resulting in difficulty to realize their emerging optical or electronic properties. Especially, the relationship between interlayer distance and interlayer coupling remains to be investigated, due to the lack of effective technology. In this work, we have used laser shocking to controllably tune the interlayer distance between graphene (Gr) and Boron Nitride (BN) in the Gr/BN/Gr heterostructures and the strains in the 2D heterolayers, providing a simple and effective way to modify their optic and electronic properties. After lase shocking, the reduction of interlayer distance is calculated by Molecular dynamics (MD) simulation. Some atoms in Gr or BN are out-of-plane as well. In Raman measurements, G peak in the heterostructure shows a red-shifted trend after laser shocking, indicating the strong phonon coupling in the interlayer. Moreover, the larger transparency after laser shocking also verifies the stronger photon coupling in the heterostructure. To investigate the effects of the interlayer coupling of heterostructure on its out-of-plane electronic behavior, we have investigated the electronic tunneling behavior. The heterostructure after laser shock reveals lager tunneling current and lower tunneling threshold, proving unexpected better electrical property. From DFT calculations, laser shocking can modulate band gap structure of graphene in Gr/BN/Gr heterostructures, therefore the heterostructures can be implemented as a unique photonic platform to modulate the emission characters of the anchored CdSe/ZnS core-shell quantum dots. Remarkably, the effective laser shocking method is also applicable to various otherwise noninteracting 2D materials, resulting in many new phenomena which will lead science and technology to unexplored territories.

Keywords: 2D materials, graphene-BN heterolayers, interlayer coupling, electronic tunneling, Core-shell quantum dots, Lifetime tunability.

*__Correspondence:__ Prof. Gary J. Cheng, Phone: 765-494-5436, e-mail: gjcheng@purdue.edu; Prof. Lei Ye, 86 27- 87792461, e-mail: leiye@hust.edu.cn; Prof. Joseph Irudayaraj, Phone: 765-494-0388, e-mail: jirudaya@illinois.edu.

Introduction:

Owing to the dangling bond free nature and strong Young's modules of 2D materials, the random assembling of various 2D materials at atomic vertical scale is presenting an anticipated paradigm to enable properties induced by interlayer couplings between 2D materials[1-6]. However, one of the challenging roadblocks towards fabrication and implementation of such van der Waals heterostructures with expected properties, is the lack of accurate understanding of interlayer coupling and the ambiguity of promoting interlayer coupling to a significant level [6]. In order to induce strong interlayer coupling in heterostructures, two atomic layers of 2D materials need to be brought in compromised distances [6]. Nevertheless, 2D materials in general after pressed would bounce back to increase the distance between the two, if the pressure is applied slowly and pressure value is not enough. Ultrafast and high pressure shocking therefore, is the effective option to promise exciting possibilities for tuning the interlayer distance in heterostructures [7-9], however, this method often brings catastrophic damages to the target 2D materials. Thankfully, compressing laser shocking duration time to enhance the pressure is feasible [10, 11], and the nature of non-contacting with other matters is completely different with other matter pressure methods, which is free from contaminations, as a result, it is possible to study the compact relationship between interlayer distance and interlayer coupling in 2D materials-based heterostructures. Laser shocking method used to study interlayer coupling in heterostructures would be a breakthrough invention as there is no report or even an attempt in this direction till date. Dedicated studying along this direction is poised to help in practical realization of several future generations of functional devices which potentially will employ heterostructures of 2D materials.

In this paper, we report the effect of laser shock on the interlayer couplings between graphene and BN in the Gr/BN/Gr heterostructures. After laser shocking, the contaminations and wrinkles induced by transfer methods can be overcome to eliminate the undesirable interferences for interlayer couplings. Molecular dynamics (MD) simulations have been carried out to get a glimpse of the laser shocking effect on the reduction of interlayer distance between Gr and BN, which also indicate the standard

flat structures of Gr and BN to be out-of-plane. To further verify the enhanced interlayer coupling strength, a series of electronic and optical properties have been studied. Raman spectroscopy has been utilized to get quick information of phonon interlayer couplings induced by laser shocking, while optical transparency measurements indicate strong photon-matter interlayer couplings. The enhanced electronic tunneling and lowered tunneling threshold across Gr/BN/Au heterostructures, prove the modulated electron transport behavior attributed by the reduction of interlayer distance. Moreover, from density functional theory (DFT) calculations, molecular orbitals of Gr and BN in close proximity will hybridize to modify electronic band structure of Gr after laser shocking. From emission characters of PbTe/ZnS core-shell quantum dots anchored on Gr/BN/Gr heterostructures before and after laser shocking, the enhanced emission lifetime is also a convincing evidence for strong interlayer couplings. Significantly, the novel laser shock method is a powerful way for vertical structure modulation, and opens up a new route for deeper understanding in quantum coupling strengthen based on various 2D heterolayers.

Results and discussion

High-quality graphene and h-BN were obtained by Chemical vapor deposited (CVD), both free from oxygen-functionalities on their surface. Then, various heterostructures including Gr/BN and Gr/BN/Gr were fabricated by wet chemical transfer method (indicative schematic of the detailed process of wet chemical transfer as shown in Fig. S1). During the transfer process, polymer contaminations such as PMMA can harm optical and electronic properties of graphene, and contaminations also will block the reduction of interlayer distance, and act as scattering centers to disturb device performances [12, 13]. To better understand the laser shocking enhanced interlayer coupling, we have carefully fabricated the heterostructure, and PMMA residues have been removed completely, according to XPS results shown in Fig. S2. However, wet chemically transferred single-layer Gr and BN onto substrates such as cover slip, silicon and gold, would still leave behind lot of wrinkles and voids at the surface and interfaces, which can be reduced upon mild heating at 80 ℃ for 20 minutes but cannot be ruled

out completely. Formation of such wrinkles can be traced to the presence of air at the interface and strain effect when such multilayer stack is transferred to the substrate[14]. These wrinkles and voids can lead to strong scattering, and the interlayer couplings in the heterostructures are disturbed severely, therefore for further investigation of the interlayer couplings, it's urgent to flatten the undesired wrinkles and voids and remove surface contaminations [14-16]. In this study, laser shocking has been used to tune the interlayer distance and the in-plane strains in the 2D layers (schematic diagram shown in Fig. 1(a)). The laser shocking in an ultrashort time scale (tens of picosecond) can produce a stress up to ~20 GPa-level at the pulse peak, then the laser power is diffused and the stress is decreased slightly, but the stress can still at ~ 15 GPa level, (Fig. 1(b), which is much higher than traditional methods, such as most recent Dean group's work [6], they have applied piston-cylinder pressure cell, but the pressure is lower than 2.4 GPa. More importantly, the strains in the multiple 2D-layers remain after laser shocking while the strain after piston-cylinder compression does not hold after the deformation which can be a problem in real application. Thus by applying our laser shock method, the ultrafast and high pressure is effective to flatten the wrinkles and voids without any damage to the heterostructures (Fig. 1(a), inset), which can be observed through AFM images (Fig. 1(d)-(g)). Laser shocking not only does flattening of the remaining wrinkles and voids presenting at interface, it also brings the reduction of distance between Gr and BN (Schematic is shown in Fig. S3 in the Supplementary Materials). Since the stress is up to ~20 GPa, the interlayer distance can be reduced effectively. To evaluate the lattice structure evolution after laser shock, first principle calculations are conducted. As shown in Fig. 1(c), in the Gr/BN/Gr heterolayer, all three layer bear large lattice strain with obvious difference, both intra- and inter- layer lattice mismatch is modulated distinctly, which is the origin of coupling modulation [17-19]. Since the interlayer couplings are of van der Waal nature ($F_{12} = A/r^6-B/r^{12}$), even weak change in interlayer distance will have dramatic impact on interlayer couplings.

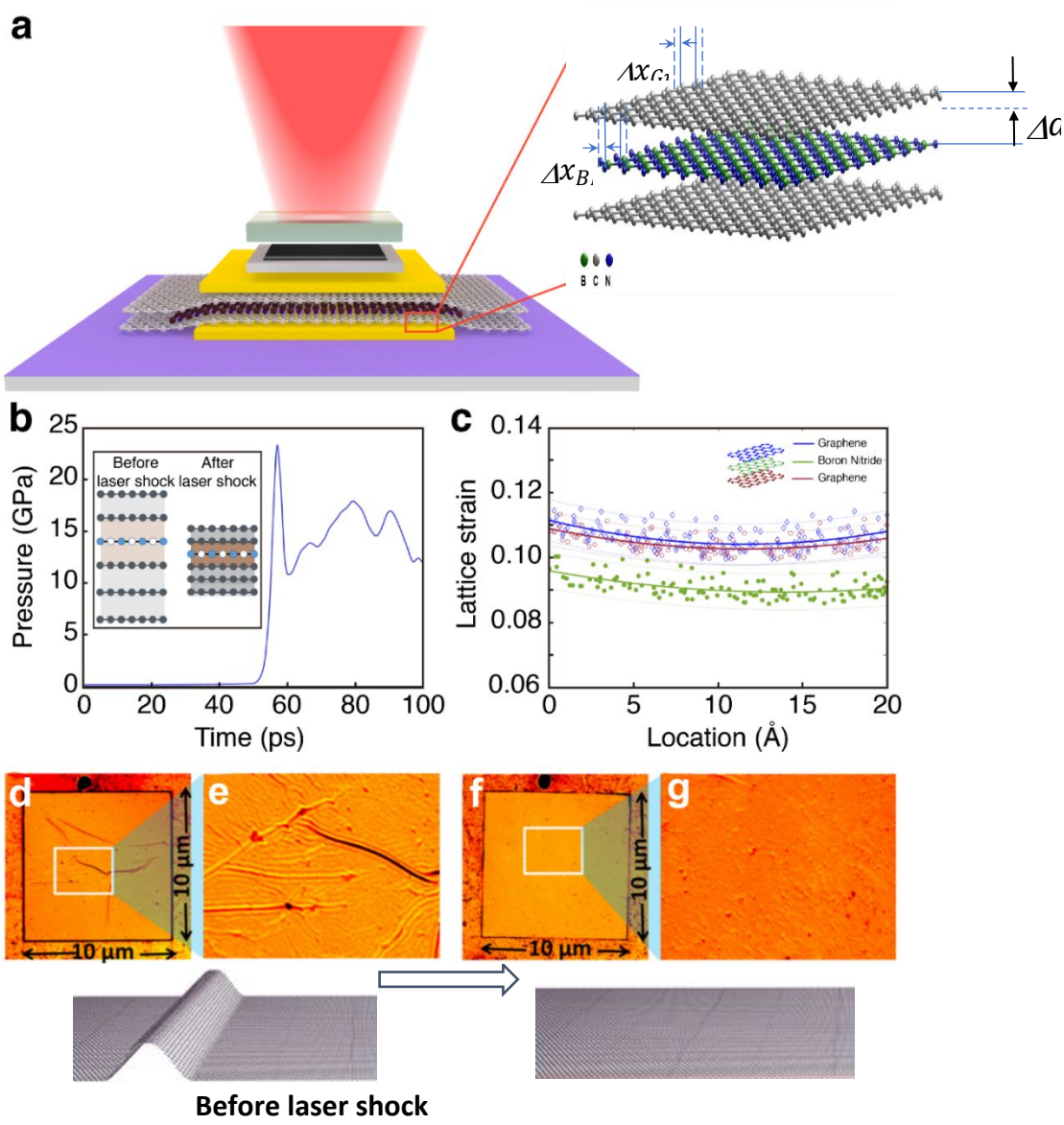

Fig 1. (a) Schematic diagram of laser shock experimental setup. Schematic diagram of wrinkles on graphene after wet transfer and (e) flattened graphene after laser shock. (b) Transient laser pressure evolution, the laser pulse generates a high pressure of ~23 GPa, then the pressure is decreased slightly due to the energy diffusion, but the pressure is still rather high at the level of ~15 GPa. The high pressure is a record in the field of laser shock engineering, which is bound to modulate the materials interaction severely. The inset shows the schematic of decreased interlayer distance of graphene/BN/graphene heterolayer, indicating that the interlayer coupling is increased. (c) First principle calculations for the lattice strain distribution. The strain in top graphene, BN and bottom graphene shows obvious difference, the intralyer strain also changes slightly. Such strain difference changes both intra- and inter- layer lattice mismatch, so the coupling strength is modulated effectively, which is bound to change the optics and electrical properties of the heterolayer. The inset shows the heterolayer structure. (d)-(g) Optical microscopy images for top graphene surface before [(d) and (e)] and after [(f) and (g)] shock to the Gr/BN/Au device stacks. Zoomed-in optical

images of wrinkles are shown in (e) before and (g) after laser shock. The wrinkles are removed completely after ultrafast and high pressure laser shock.

To explore the impact induced by laser shocking, MD simulation is used to reveal the formation mechanism of Gr/BN/Gr heterostructure which is applied by a GPa-level pressure within picoseconds, as shown in Fig. 1(b). Based on the results, the in-plane structures of Gr and BN are evolved to be out-of-plane, and the interlayer distance of out-of-plane structures indeed reduces, due to laser shocking inducing compression in Z-direction for the heterostructure, resulting in ~0.4 eV band gap opening of the heterostructure from DFT results (Fig. 2(a) and 2(b), mid and right column). Laser shocking induced ultrahigh pressure with ultrafast strain rate can provide the permanently compressed configurations for the heterostructure to bring p_z orbitals close proximity, leading to the enhancement of interlayer coupling (Fig. S4 and S5, Supplementary Materials) between Gr and BN (level "UP" interlayer coupling).

On the other hand, the enhanced interlayer couplings induced by laser shocking can also be presented from the Raman spectrum of the heterostructures. Studying the Raman spectrum of graphene in the heterostructures, the G peak signal is originated from the in-plane vibrational E_{2g} phonon due to sp^2 bonded carbon atoms in a hexagonal ring, which possesses six carbon atoms to form two sublattices vibrating in opposite directions. Raman peak shifts can be related with many factors, such as layer thickness, substrate, defects, contamination, temperature and lattice strain [12, 20-22]. Here we can rule out the influence of layer thickness, substrate and temperature. We have used high quality graphene, and the laser shocking is not directly illuminated on graphene because aluminum foil is placed above the sample, so the influence of defects can be ignored. After graphene transfer, we have removed the contaminations on the sample to eliminate its influence. Finally, the most probably reason is strong interlayer coupling, since the laser shocking induces ultrahigh stress in a short time to reduce of the interlayer distance effectively. After laser shocking, the enhancement of out-of-plane atomic coupling and the reduction of interlayer distance will make the total energy of the heterostructures increased. To release the total energy, it is required to soften the

in-plane interactions with expanded in-plane lattice, so the covalent bonds in the two sublattices becomes weaker, leading to the red-shift of G peak [17-19]. According to Raman measurements, the results of graphene, BN atomic sheet, and Gr/BN/Gr heterostructures with/without laser shocking are shown in Fig 2(c), respectively. For graphene, it exhibits Raman signal peaks at ~1380 cm^{-1}, 1587 cm^{-1} and 2645 cm^{-1}, corresponding to D, G and 2D peaks. After laser shocking, the D peak with little change means that graphene sheet is not degraded after laser shocking. The G peak of graphene is observed to be little red-shifted for Gr/BN/Gr heterostructure compared with graphene, which is induced by BN. Interestingly, there is a strong red-shifted of 2D peak after laser shocking, proving the strong interlayer coupling induced by laser shocking to modify the optical property of 2D materials-based heterostructures. The transparency as an important optical property of graphene is over ~96% in the range of below 3.5 eV photon energy (as shown in Fig. 2(d)), but the fast decrease is observed in the range over 3.5 eV. The distinct absorption of graphene in high photon energy range can be attributed to resonant excitonic effects, where electron and hole interacts in the π and π^* bands at the M point of the Brillouin zone in graphene lattice. In Gr/BN/Gr heterostructure, the three-layer structure increases the photon absorption, thereby showing a lower transparency than that of graphene. After laser shocking, the interlayer distance and coupling are enhanced to generate a small bandgap in the heterostructure, and the bandgap energy barrier will impede photon absorption, leading to higher transparency than that of the heterostructure without laser shocking. To further verify the bandgap opening, we have also measured the absorption spectra in the infrared region (0.2 eV to 0.6 eV), as shown in the inset of Fig. 2(d). Before laser shocking, strong absorption in the range of 0.2 eV to 0.6 eV is observed, however, after laser shocking, the absorption edge is blue-shifted to ~0.4 eV. For energies below 0.4 eV, the absorption is not observed obviously, which indicates that the large bandgap of graphene is opened.

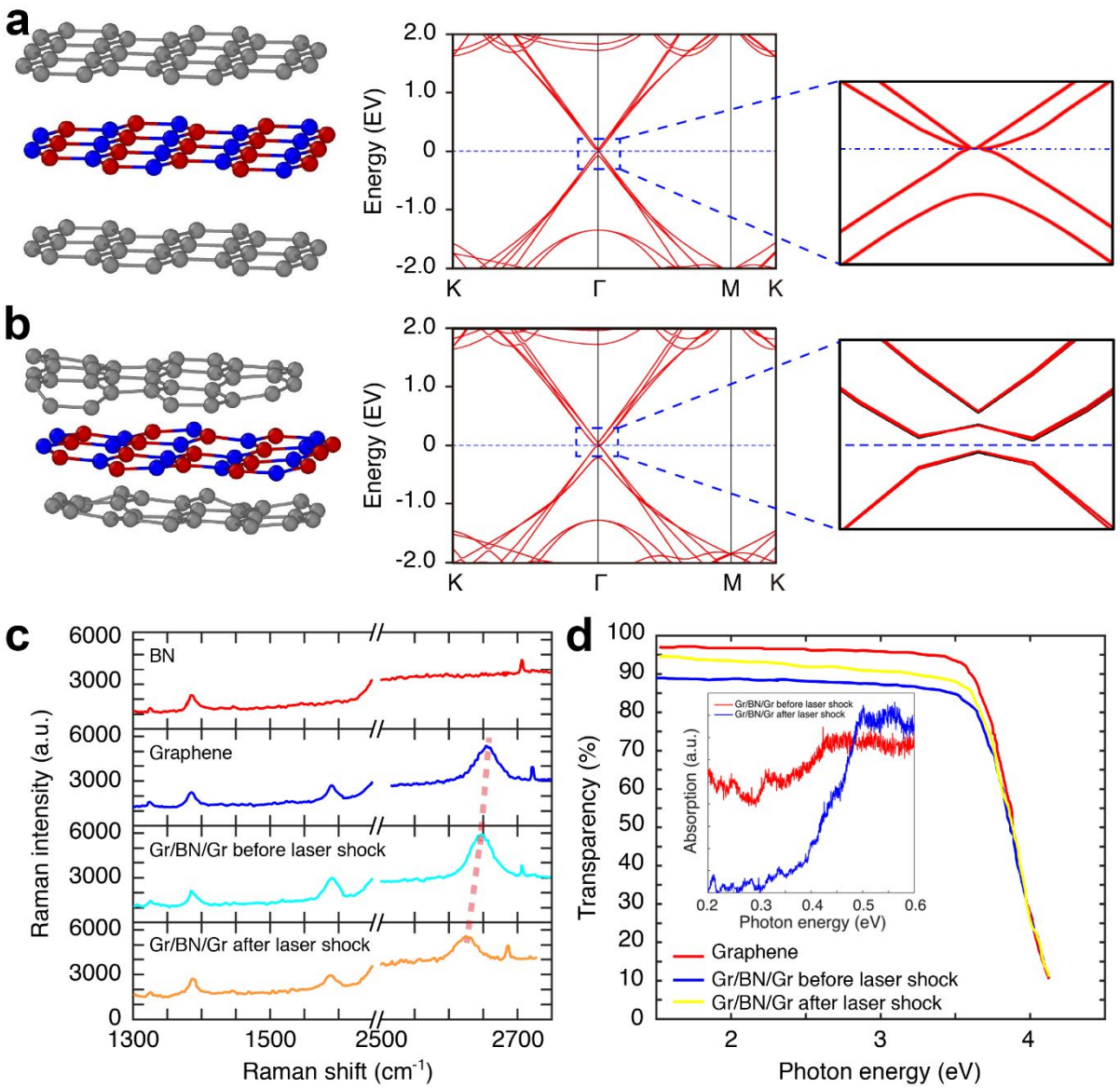

Fig 2. (a)-(b) DFT Band structure calculations for graphene/BN/graphene heterolayer (a) before and (b) after laser shock. The first column shows schematic of the heterolayer, with enhanced intralayer lattice mismatch and reduced interlayer distance, which is the origin of modulated coupling. The second column shows corresponding calculated band structures, the third column shows zoomed-in version of the band structure in close proximity of Γ-points, after laser shock, a large band gap is emerged. (c) Raman spectra and (d) UV-VIS spectra for graphene, BN, and graphene/BN/graphene heterolayer before and after laser shock. The Raman G peak is red shifted after laser shock, and the transparency is enhanced too. The inset of (d) shows absorption spectra of the heterolayer in the range of 0.2 eV to 0.6 eV photon energy.

We have also designed Gr/BN/Au heterostructure to study the electronic tunneling behavior, illustrating strong interlayer coupling induced by laser shocking to modulate electronic property of 2D materials-based heterostructures, as shown in Fig. 3(a). The tunneling barrier is uniform monolayer BN. In order to deeply investigating this tunneling process, we have carried out experiments to test the bias dependence of *I-V* curve, with various bias from -50 to 50 V (Fig. 3(d)-(e)), there is steady increase in tunneling current with applied bias for positive bias region, which is mainly originated from direct tunneling through BN layer. However, in negative bias region, the tunneling current increases rapidly when the bias is lower than a bias threshold, and this large tunneling current is attributed to Fowler-Nordheim (FN) tunneling mechanism. Based on FN tunneling mechanism, potential barrier is tilted with triangular shape under extreme negative bias (Fig. 3(b)-(c)), so the tunneling current increases sharply [23]. In Fig. 3(d), the tunneling current in the negative bias region is much larger than that of in the positive bias region. The differential conductance before and after laser shocking is shown in Fig. 3(e). To verify the tunneling mechanism in this metal-insulator-semiconductor junction, we have calculated the tunneling current based on FN model[36], by using equation(1) [23]:

$$J_{FN} = C_{FN} \times V^2 \exp\left(-\frac{4\sqrt{2m_{BN}^*}(qf_B)^{\frac{3}{2}}}{3q\hbar V}\right), \quad (1)$$

where m_{BN}^* is the effective electron mass, q is the electron charge, $\hbar$ is the Planck constant, f_B is the tunneling barrier, and C_{FN} is a constant. Remarkably, the tunneling current of the sample with laser shocking (Fig. 3(d), blue line) is distinctly higher than that of the sample without laser shocking (Fig. 3(d), red line). In this mechanism, electrons do not directly tunnel from graphene to Au electrode across the barrier, instead, they can tunnel from graphene to the conduction band of BN, and then relaxing to Au electrode, the domination in this process is the barrier between graphene and BN. Thus, the larger tunneling current in laser shocking heterostructure is attributed to the lower barrier between graphene and BN (Fig. 3(b)-(c)), which is originated from reduced interlayer distance and enhanced interlayer couplings. Furthermore, the diode-like *I-V* behavior becomes more prominent after laser shocking, presumably due to the

interface passivation. To quantitively verify the mechanism transition from direct tunneling to FN tunneling and the tunneling barrier changes after laser shocking, Fowler-Nordheim plot ln ($I(V)/V^2$) vs $1/V$ is plotted for BN/Graphene-based heterostructure tunneling device before and after laser shocking process (Fig 3(f)) [23].

$$\ln\left(\frac{1}{C_{FN}} \times \frac{J_{FN}}{V^2}\right) = -\frac{4\sqrt{2m_{BN}^*}}{3q\hbar} \times (qf_B)^{3/2} \times \frac{1}{V}. \quad (2)$$

Three distinguishable regions of applied bias are observed in experimental curves (shown in golden, red and blue shades). The blue shaded range of applied bias shows logarithmic shape, which is due to direct tunneling mechanism. In the red shaded range, direct tunneling and FN tunneling are competing due to larger electric field in the heterostructure. The gold shaded region possesses largest applied bias, and FN tunneling mechanism dominates in this region, the curve shows a linear line shape [23]. As is obvious from the slopes of the tangents drawn in this tunneling regime (Fig 3(f)), before laser shocking, the tunneling threshold bias is ~-12.5 V, however, a lower applied bias of ~-7.8 V is needed to switch the tunneling ON after laser shock. The enhanced interlayer coupling and reduced interlayer distance, with minimum defects in BN crystal and electronically smooth interfaces between Gr and BN have lowered the unwanted carrier scattering, which induced by huge laser shocking, are responsible for the excellent tunneling performance.

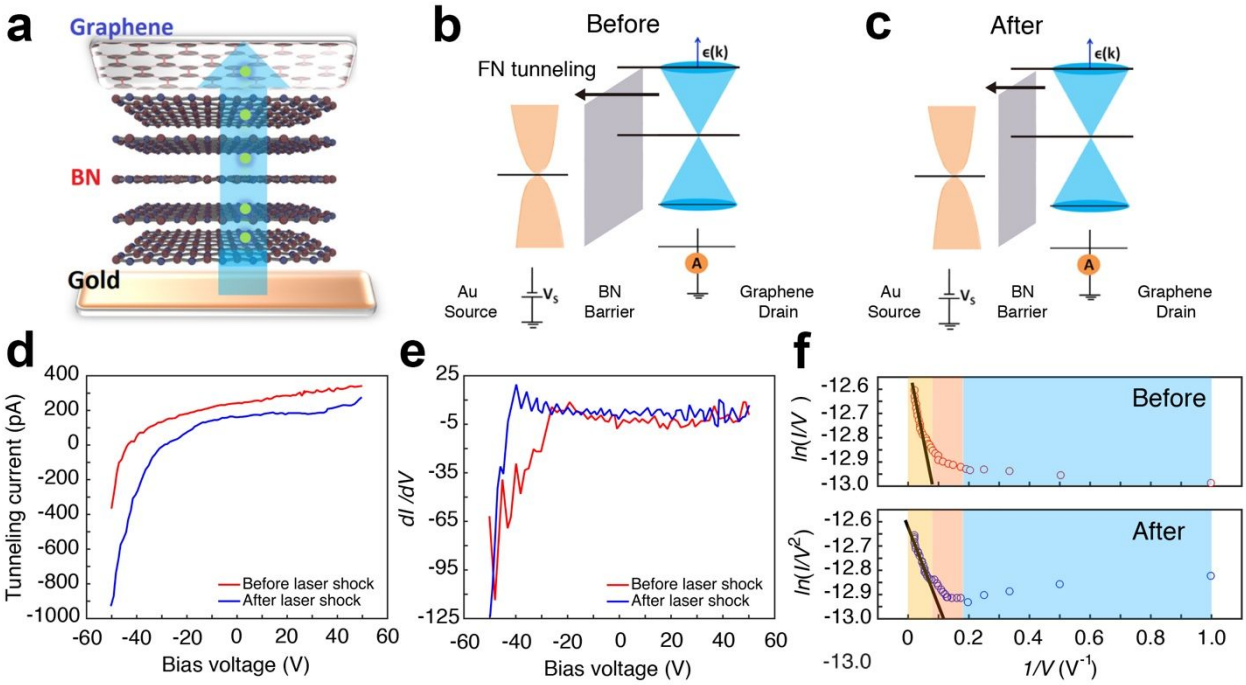

Fig 3. (a) Schematic diagram of Gr/BN/Au tunneling heterolayers. (b) and (c) are schematic diagrams of the FN tunneling before and after laser shock, respectively. Under extreme field limit, rectangular effective potential barrier becomes triangular which result in huge tunneling current. (d) I-V characteristic for Gr/BN/Au heterostructure tunneling device with bias voltages ranging from namely - 50 V to +50 V before (red line) and after (blue line) laser shock, and (e) the corresponding tunneling conductance before (red line) and after (blue line) laser shock. The tunneling current is increased after laser shock. (f) Fowler-Nordheim plot [(ln I/V^2) vs. 1/V] before and after laser shock. When bias is gradually elevated (as one moves towards left) three distinctly different regimes in plot is apparent. Rightmost blue region represents negligible tunneling regime, middle red region represents transition region and leftmost gold region represents huge tunneling at extreme field values. After laser shock, the tunneling threshold is reduced effectively, indicating that carriers are easier to tunnel through the barrier.

The laser shocking induced bandgap opening of graphene in the Gr/BN/Gr heterostructure, gives rise to a large electron effective mass near the Dirac point in graphene, so the electron-photon interaction between the heterostructure and other 0D-3D materials is modified after laser shocking. To evaluate the capability of the Gr/BN/Gr heterolayers in engineering the local photonic density, we have characterized the electron-photon interaction of the single CdSe/ZnS quantum dots (QDs) located on coverslip, graphene and Gr/BN/Gr heterostructures before and after laser shocking, respectively. Fig. 4(a) shows the time-course fluorescence emission from single QD in coverslip, no carrier transfer occuring between QDs and the substrate, so the nonradiative decay is suppressed. When QDs are transferred to graphene (Fig. 4(b)), it shows the strong carrier transfer from the QDs to the graphene due to its zero bandgap nature, to enhance the nonradiative decay rate of the QD by more than 10 times [24-27]. For Gr/BN/Gr heterostructure before (Fig. 4(c)) and after laser shocking (Fig. 4(d)), the reduction of fluorescence intensities for QDs can both also be observed, but the intensities on them are much stronger than on graphene due to the existence of bandgap. Since the interlayer coupling after laser shocking is enhanced, the induced larger bandgap impedes carrier transfer between QDs and graphene in the Gr/BN/Gr heterostructure, the fluorescence emission intensity is stronger than that of the heterostructure without laser shocking (Fig. 4(d)). Emission lifetime of QDs also gets altered due to localized light-matter interaction for different structures [28, 29]. Fig. 4(e)-(h) have shown the photon emission lifetimes of QDs on coverslip, graphene, and Gr/BN/Gr heterostructures before and after laser shocking, respectively, suggesting relatively long lifetime of QDs induced by laser shocking. The time-correlated single photon counting (TCSPC) decay curves are measured in Fig. 4(i). Because the coverslip and QDs have no photon-mater interactions, the decay time is rather long. On graphene substrates with zero bandgap, the decay time is much shorter due to strong carriers transfer from QDs to graphene. But for BN, it is an electrical insulating material, thus the local photonic density of QDs cannot be significantly changed by BN, the decay time is close to the coverslip (Fig. 4(j)). However, compared with QDs on the graphene with an averaged fluorescence lifetime of 5.47±1.24 ns, QDs on the Gr/BN/Gr exhibit

an averaged fluorescence lifetime of 5.81±1.26 ns without laser shocking. The slightly higher fluorescence lifetimes for the Gr/BN/Gr heterostructure without laser shocking, indicates that there is only limited impact in the heterostructure. After laser shocking, the averaged fluorescence time is increased to 7.51±2.49 ns, and the much higher lifetime is attributed to the enhanced strong interlayer coupling between graphene and BN sheet. This phenomenon also suggests that the graphene-BN coupling is much localized after laser shocking, and then is vanishing quickly along the longitudinal direction. Finally, we have systematically analyzed the spontaneous fluorescence decay by quantifying the lifetime components and their amplitudes with a multi-component exponential decay model:

$$I(t) = I_1 \times \exp\left(-\frac{t}{\tau_1}\right) + I_2 \times \exp\left(-\frac{t}{\tau_2}\right) \qquad (3)$$

QDs on the coverslip possess fast components of ~3.10 ns and a slow component of ~15.27 ns with 25.6% and 74.4% amplitude for each component. The strong light-matter interactions between QDs and Gr/BN/Gr heterostructure can generate an even faster decay component after laser shocking, ~0.7 ns, which is comparable with the time of the Auger process (0.5-0.7ns) [30], and this is the reason for multiphoton emission from QDs on the laser shocking Gr/BN/Gr heterostructures.

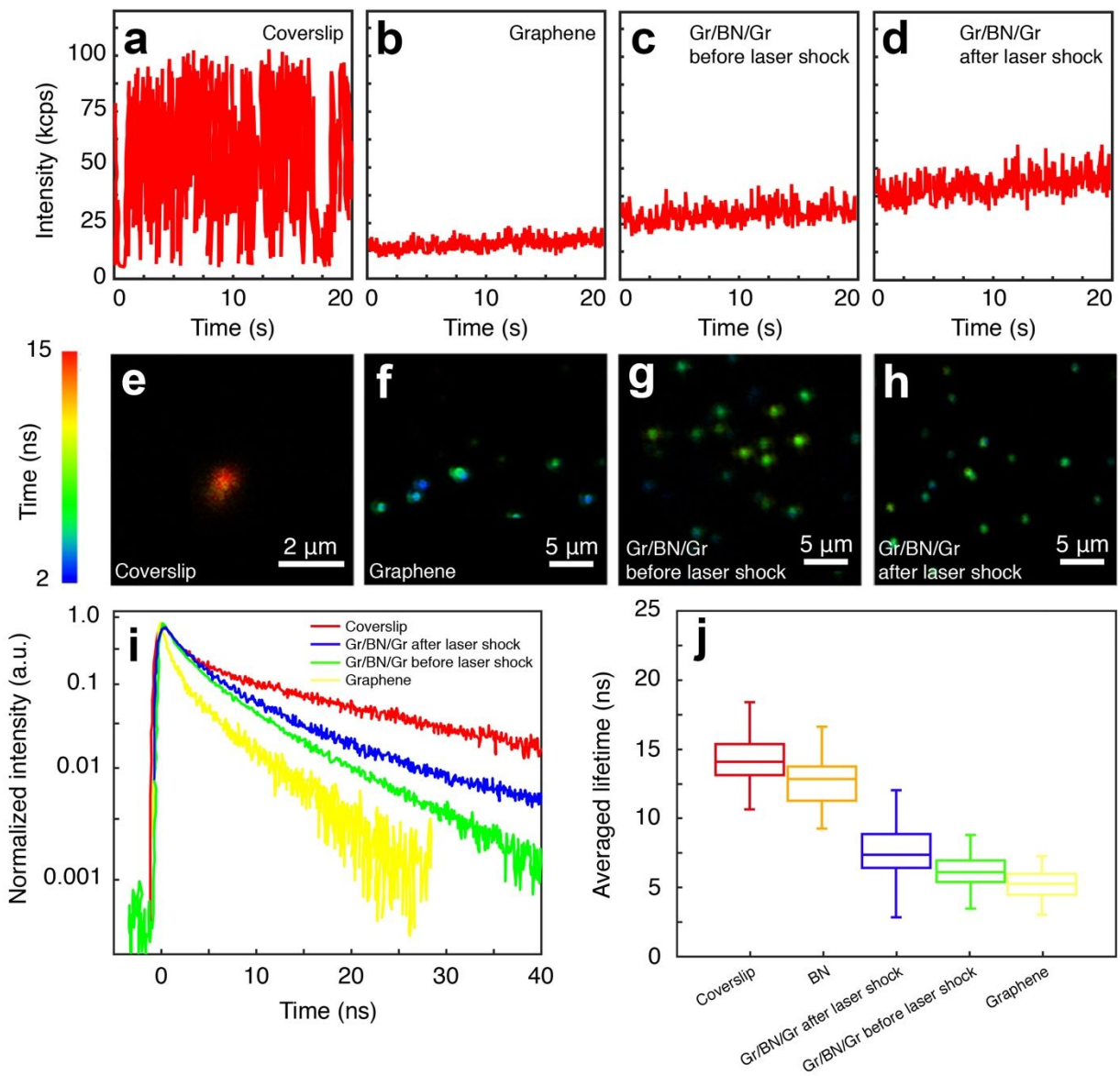

Fig 4. Photon emission behavior of QDs in presence of different photonic states. (a) Time-course fluorescence emission from single QD suggests significant "blinking" on coverslip, which was inhibited on Gr/BN/Gr heterolayers. (b)-(d) Time-course fluorescence emission from single QD on bare graphene (b), and Gr/BN/Gr heterolayer before (c) and after (d) laser shock. (e-h) Fluorescence-lifetime imaging microscopy (FLIM) images of QDs on (e) coverslip, (f) Graphene, Gr/BN/Gr before (g) and after (h) laser shock. (i) Time-correlated single photon counting (TCSPC) decay curves of single QDs on different substrates. (j) Statistical summary of fluorescence lifetimes of individual QDs on different substrates. A larger bandgap after laser shock can increase the fluorescence lifetime.

It's also worth to be noted that our laser shocking method is feasible for a wide range of materials, including CVD or epitaxial grown heterostructures. The CVD or epitaxial grown heterostructures are free from wrinkles, but to further enhance

interlayer coupling is still obstructed due to Coulomb interactions. By applying laser shocking to these heterostructures, it's bound to induce more unique properties with enhanced interlayer interactions, which is worth investigating.

In conclusion, we have employed laser shocking for the first time to integrate and hybridize 2D materials (graphene and BN). This method can not only eliminate the bubbles/voids produced by the constructed process of 2D materials-based heterostructure and flatten atomic sheets of 2D materials, but also induce the strong interlayer couplings to modify their optical or electronic properties. We have verified this issue from the new phenomena of in-plane vibrational phonon, emergent bandgap opening, and quantum electronic tunneling, which are all induced by laser shocking. The ultrahigh laser shocking pressure and strain rate, are effective to suppress interlayer distances and tune interlayer couplings, suggesting that a promise of various new quantum interlayer phenomena in 2D vdW heterostructures becomes experimentally accessible.

Methods

1. Heterolayer structure fabrication for electronic tunneling measurements

Photolithography was carried out using photomask having square shaped (10μm x 10μm) openings to achieve pillared patterns, each pillar having dimensions 10μ x 10μ. Photolithography was followed by e-beam deposition of Ti-Au to achieve the stack having configuration Au(100 nm)/Ti(50 nm)/SiO_2(300 nm)/Si. Single layer graphene (SLG) and multilayered BN (MLBN) (6 nm) grown on copper (NanoLab Inc., Waltham, MA, USA) by chemical vapour deposition (CVD) were used to fabricate multilayer stack. Details of wet chemical transfer are presented in Fig S1. Top surface of Gr/Cu was coated with 100 nm of PMMA (Sigma Aldrich) and baked for 20 minutes at 60 ℃. Copper substrate was dissolved in aqueous solution of $FeCl_3$. After copper substrate is dissolved, PMMA/Gr is transferred to distilled water, after 30 minutes,

sample is transferred to another Petri-dish having fresh distilled water and the process was repeated again and again till even after keeping for 30 minutes water does not become yellowish at all. Top surface was cleaned by acetone first, followed by cleaning in toluene. To prepare Gr/BN sample, PMMA/Gr is transferred to properly cleaned BN coated Cu sheet, and dried overnight. Thus PMMA/Gr/BN/Cu was achieved and Cu substrate was again dissolved in $FeCl_3$ aqueous solution and appropriately transferred multiple times in separate Petri-dishes having D.I. water. Finally, PMMA/Gr(1L)/BN(6 nm) was transferred to already fabricated Au(100 nm)/Ti(50 nm)/SiO_2(300 nm)/Si. After adequately drying, Gr/BN multilayer stack sticks well with the existing stack. After the final transfer of stack on the substrate, PMMA was cleaned using acetone followed by toluene. After adequate drying, conducting Au/Ti layer was coated on the top. After the conducting layer coating on the top, plasma etching was carried out on the final stack to electronically isolate fabricated pillars.

2. MD Simulation Details

Non-equilibrium molecular dynamics (NEMD) simulations were performed by using the Large-scale Atomic/Molecular Massively Parallel Simulator (LAMMPS) [31] to understand the effect of laser shock pressure on the inter layer distance for the graphene-BN heterolayers. Open visualization Tool (OVITO) [32] was used to post process the data obtained from MD simulation. The G/BN/G heterostructure was modeled with help of VESTA [33] with flake dimensions of 20 Å x 20 Å. Tersoff potentials [34] adopted from Kinaci et al.[35] was used to define the intralayer B-N interatomic force fields and the second-generation reactive empirical bond order (REBO) potential [36] is used to define the intralayer GNR interactions. Lennard Jones potential was used to define the non-bonded interactions between carbon, boron and nitrogen atoms [37] which is described as, $V=4\epsilon[(\sigma/r)^{12}-(\sigma/r)^{6}]$, where ϵ and σ are the potential parameters which were calculated using Lorentz-Berthelot mixing rule [36]. It is important to note that the short range interactions between boron-boron atoms were neglected because the Van der Waal's radius for boron (192 pm) is much smaller than the distance between the BN layers (330 pm) [36]. Energy minimization was carried out on the meta-layer configuration followed by equilibration under isothermal isobaric

(NPT) ensemble with time step of 0.5 fs for 50 ps. A force equivalent to 10 GPa laser pressure was applied to the heterolayer under NVT ensemble with time step of 0.1 fs to obtain the equilibrated laser shocked structure. The co-ordinates of the laser shocked heterolayer were further extracted to further perform DFT calculations.

3. Details of laser shock processing

Graphite coated (Asbury Carbons, USA) 4 μm thick aluminum foil (Lebow Company, USA) was placed on the top of Gr (1 L) / BN (ML, 6 nm) multilayered stack placed on Au (100 nm)/Ti(50 nm)/ SiO_2 (300nm) /Si substrate. A fused silica was placed on top of the graphite coating to confine and enhance plasma expansion. A Q-switch Nd-YAG laser (Continuum® Surelite III) (1064 nm wavelength and 5 ns pulse duration) was used to irradiate the sacrificial layer. Intense laser instantaneously evaporates the graphite layer and ionized plasma and strong momentum was generated. The shock wave was then transferred onto the target sample. Laser shock instantly flattens the remaining ripples/wrinkles/voids present at surface/interfaces.

4. Strain calculation in the heterostructure

Displacement field in continuum crystal plasticity was defined at every material point. Stukowski and A. Arsenlis[38] developed a technique to define an atomistic displacement field using linear interpolation for molecular dynamics in which the bond vectors were mapped to neighboring atoms to derive a stress-released state. The atomic lattice strains were calculated with help of the local deformation gradient tensor for each particle from relative displacements of the neighbors of the particles[39]. The Green Lagrangian strain tensor E was calculated by using the atomic deformation gradient tensor F given by, $= 1/2(F^T - I)$, and the stretch tensor U was calculated by decomposing the atomic deformation gradient, $F=RU$, where, R is the rotation matrix. The layer-wise lattice strains were calculated at the deformed shocked G/BN/G configuration, plotting along the location, as shown in Fig S1. The lattice strains in graphene layers were ~11% and the strain in the boron nitride layer was found to ~9%.

5. Microscopy and spectroscopy

Optical imaging was acquired in Olympus microscope at magnification up to 100x. A Raman spectrometer (Bruker Senterra) equipped with near-infrared laser (λ = 785 nm)

was used for acquiring Raman signatures of graphene, BN and Graphene/ BN heterolayer on plasmonic gold nanoparticles.

6. Tunneling measurements

Probe Station used in tunneling measurements consists of a Micromanipulator 6000 in a dark box on top of a vibration isolation table. Keithley SCS4200 test equipment was used for the purpose having an HP 4284A LCR meter. A Windows-NT PC running Labview is used to drive the instruments and collect the data.

7. Lifetime measurements and G2 measurements:

CdSe/ZnS QDs (Q21721, Invitrogen, CA, US) was first decane-diluted in poly(methylmethacrylate) (PMMA) with a volume ratio of 1:10,000, and then spin-coated on metamaterial samples to achieve mono-dispersion. The photon emission behavior of the QD was evaluated in a fluorescence lifetime imaging microscopy (FLIM). A picosecond pulsed laser (467nm, 20 MHz) was delivered to a water-immersion objective (Olympus, 60X, 1.3 N.A.) for excitation. Fluorescence signal from individual QDs was first filtered by a dichroic mirror and band-pass filters, then split by a 50/50 beam-splitter, and finally collected by two single-photon avalanche photodiodes (SPAD) (SPCM-AQR-14, PerkinElmer Inc.). The photons were recorded in a time-tagged-time-resolved mode. Fluorescence lifetime was obtained by fitting the time-correlated single photon counting (TCSPC) decay curve with a multi-component exponential decay function, and the photon emission statistics was recorded by a Hanbury Brown-Twiss setup and was evaluated by the second-order autocorrelation function $G2(\tau)=\langle I(t)I(t+\tau)\rangle/\langle I(t)\rangle^2$. Details about the instrument and analysis can be found in our previous reported works[25,40].

8. Band structure calculations:

To calculate the electronic properties of these systems, spin polarized density functional theory (DFT) methods as implemented in SIESTA package[45] with PBE/DFT-D2[46] exchange correlation functional has been used. We have used 4 X 4 supercells for all the calculations. We have used a vacuum of 20 Angstrom in the nonperiodic direction to avoid any unwanted interactions.

Acknowledgements:

Financial assistance in the form of National Research Council Senior Research Associateship (G.J.C.), and NSF Grant Nos. CMMI-0547636 and CMMI 0928752 (G.J.C.) has been crucial for these experiments. PK acknowledges financial support from Science and Engineering Research Board, Dept. of Sci. and Tech., Govt. of India in the form of The Ramanujan Fellowship (sanction no. SB/S2/RJN-205/2014). AB thanks TUE- CMS for computational facilities.

Contributions of Authors:

GJC conceived the concept. PK carried out metalayer fabrication; YH helped in sample characterizations, JL transferred quantum dots on its top surface and carried out emission lifetime measurements on it. PK then fabricated electronic tunneling devices and carried out electronic tunneling measurements. MM conducted MD simulation. AB carried out band structure calculations under supervision of SKP. LT, XH, and LY analyzed the results. PK, LY, and GJC wrote the paper. JI and GJC oversaw the project.

Conflicts of interest

Authors declare no conflicts of interest.

References:

1. Lee, C.-H.; Lee, G.-H.; Zande, A. M. v. d.; Chen, W.; Li, Y.; Han, M.; Cui, X.; Arefe, G.; Nuckolls, C.; Heinz, T. F.; Guo, J.; Hone, J.; Kim, P., Atomically thin p–n junctions with van der Waals heterointerfaces. *Nat. Nanotech.* **2014,** *9*, 676-681.

2. Bediako, D. K.; Rezaee, M.; Yoo, H.; Larson, D. T.; Zhao, S. Y. F.; Taniguchi, T.; Watanabe, K.; Brower-Thomas, T. L.; Kaxiras, E.; Kim, P., Heterointerface effects in the electrointercalation of van der Waals heterostructures. *Nature* **2018,** *558*, 425-429.

3. Chen, Y.; Wang, X.; Wu, G.; Wang, Z.; Fang, H.; Lin, T.; Sun, S.; Shen, H.; Hu, W.; Wang, J.; Sun, J.; Meng, X.; Chu, J., High-Performance Photovoltaic Detector Based on MoTe2/MoS2 Van der Waals Heterostructure. *Small* **2018**, 14, 1703293.

4. Kang, K.; Lee, K.-H.; Han, Y.; Gao, H.; Xie, S.; Muller, D. A.; Park, J., Layer-by-layer assembly of two-dimensional materials into wafer-scale heterostructures. *Nature* **2017,** *550*, 229-233.

5. Unuchek, D.; Ciarrocchi, A.; Avsar, A.; Watanabe, K.; Taniguchi, T.; Kis, A., Room-temperature electrical control of exciton flux in a van der Waals heterostructure. *Nature* **2018,** 560, 340-344.

6. Yankowitz, M.; Jung, J.; Laksono, E.; Leconte, N.; Chittari, B. L.; Watanabe, K.; Taniguchi, T.; Adam, S.; Graf, D.; Dean, C. R., Dynamic band-structure tuning of graphene moiré superlattices with pressure. *Nature* **2018,** *557*, 404-408.

7. Badding, J. V., High pressure synthesis, characterization and tuning of solid state materials. *Annu. Rev. Mater. Sci* **1998,** *28*, 631-658.

8. Hemley, R. J., Effect of high pressure on molecules. *Annu. Rev. Phys. Chem.* **2000,** *51*, 763-800.

9. M. C. Millan, P. F., New materials from high-pressure experiments. *Nat. Mater.* **2002,** *1*, 19-25.

10. Pezeril, T.; Saini, G.; Veysset, D.; Kooi, S.; Fidkowski, P.; Radovitzky, R.; Nelson, K. A., Direct visualization of laser-driven focusing shock waves. *Phys. Rev. Lett.* **2011,** *106*, 214503.

11. Li, J.; Chung, T.-F.; Chen, Y. P.; g, G. J. C., Nanoscale Strainability of Graphene by Laser Shock-Induced Three-Dimensional Shaping. *Nano Lett.* **2012,** *12*, 4577-4583.

12. Lin, Y.-C.; Lu, C.-C.; Yeh, C.-H.; Jin, C.; Suenaga, K.; Chiu, P.-W., Graphene annealing: How clean can it be? *Nano Lett.* **2012,** *12*, 414-419.

13. Lin, Y.-C.; Jin, C.; Lee, J.-C.; Jen, S.-F.; Suenaga, K.; Chiu, P.-W., Clean transfer of graphene for isolation and suspension. *ACS Nano* **2011,** *5*, 2362-2368.

14. Hu, Y.; Lee, S.; Kumar, P.; Irudayaraj, J. J.; Cheng, G. J., Water flattens graphene wrinkles: laser shock wrapping of graphene onto substrate-supported crystalline plasmonic nanoparticle arrays. *Nanoscale* **2015,** *7*, 19885-19893.

15. Gao, H.; Hu, Y.; Xuan, Y.; Li, J.; Yang, Y.; Martinez, R. V.; Li, C.; Luo, J.; Qi, M.; Cheng, G. J., Large Scale Nanoshaping of Ultrasmooth 3D Crystalline Metallic Structures. *Science* **2014,** *346*, 1352-1356.

16. Lee, S.; Kumar, P.; Hu, Y.; Cheng, G. J.; Irudayaraj, J. J., Graphene laminated gold bipyramids as sensitive detection platforms of antibiotic molecules. *Chem. Comm.* **2015,** *51*, 15494-15497.

17. Jung, J.; DaSilva, A. M.; MacDonald, A. H.; Adam, S., Origin of band gaps in graphene on hexagonal boron nitride. *Nat. Commun.* **2015,** *6*, 6308.

18. Xu, J.-R.; Song, Z.-Y.; Yuan, C.-G.; Zhang, Y.-Z., Interaction-induced metallic state in graphene on hexagonal boron nitride. *Phys. Rev. B* **2016,** *94*, 195103.

19. Decker, R.; Wang, Y.; Brar, V. W.; Regan, W.; Tsai, H.-Z.; Wu, Q.; Gannett, W.; Zettl, A.; Crommie, M. F., Local electronic properties of graphene on BN substrates via scanning tunneling Microscopy. *Nano Lett.* **2011,** *11*, 2291-2295.

20. Ferrari, A. C.; Basko, D. M., Raman spectroscopy as a versatile tool for studying the properties of graphene. *Nat. Nanotech.* **2013,** *8*, 235-246.

21. Calizo, I.; Balandin, A. A.; Bao, W.; Miao, F.; Lau, C. N., Temperature dependence of the Raman spectra of graphene and graphene multilayers. *Nano Lett.* **2007,** *7*, 2645–2649.

22. Ni, Z. H.; Yu, T.; Lu, Y. H.; Wang, Y. Y.; Feng, Y. P.; Shen, Z. X., Uniaxial Strain on Graphene: Raman Spectroscopy Study and Band-Gap Opening. *ACS Nano* **2008,** *2* (11), 2301-2305.

23. Chiu, P.-W.; Roth, S., Transition from direct tunneling to field emission in carbon nanotube intramolecular junctions. *Appl. Phys. Lett.* **2008,** *92*, 042107.

24. Cox, J. D.; Singh, M. P.; Gumbs, G.; Anton, M. A.; Carreno, F., Dipole-dipole Interaction Between a Quantum Dot and a Graphene Nanodisk. *Phys. Rev. B* **2012,** *86*, 125452-125461.

25. Liu, J.; Kumar, P.; Hu, Y.; Cheng, G. J.; Irudayaraj, J., Enhanced multiphoton emission from CdTe/ZnS quantum dots decorated on single-layer graphene. *J. Phys. Chem. C* **2015,** *119*, 6331-6336.

26. Swathi, R. S.; Sebastian, K. L., Long range resonance energy transfer from a dye molecule to graphene has (distance)(-4) dependence. *J. Chem. Phys.* **2009,** *130*, 086101

27. Chen, Z.; Nuckolls, S. B. C.; Heinz, T. F.; Brus, L. E., Energy transfer from individual semiconductor nanocrystals to graphene. *ACS Nano* **2010,** *4*, 2964-2968.

28. Anger, P.; Bharadwaj, P.; Novotny, L., Enhancement and Quenching of Single-Molecule Fluorescence. *Phys. Rev. Lett.* **2006,** *96*, 113002-113005.

29. Krachmalnicoff, V.; Castanie, E.; Wilde, Y. D.; Carminati, R., Fluctuations of the Local Density of States Probe Localized Surface Plasmons on Disordered Metal Films. *Phys. Rev. Lett* **2010,** *105*, 183901-183904.

30. Klimov, V. I.; Mikhailovsky, A. A.; McBranch, D. W.; Leatherdalde, C. A.; Bawendi, M. G., Quantization of multiparticle Auger rates in semiconductor quantum dots. *Science* **2000,** *287*, 1011-1013.

31. Plimpton, S., Fast parallel algorithms for short-range molecular dynamics. *J. comput. Phys.* **1995,** *117*, 1-19.

32. Stukowski, A., Visualization and analysis of atomistic simulation data with OVITO–the Open Visualization Tool. *Model. Simul. Mater. SR* **2009,** *18*, 015012-015019.

33. Momma, K.; Izumi, F., VESTA 3 for three-dimensional visualization of crystal, volumetric and morphology data. *J. appl. Crystallogr.* **2011,** *44*, 1272-1276.

34. Tersoff, J., New empirical approach for the structure and energy of covalent systems. *Phys. Rev. B* **1988,** *37*.

35. Çağın, A. K. B. H. S., Thermal conductivity of BN-C nanostructures. *Phys. Rev. B* **2012,** *86*, 115410.

36. Brenner, D. W.; Shenderova, O. A.; Harrison, J. A.; Stuart, S. J.; Ni, B.; Sinnott, S. B., A second-generation reactive empirical bond order (REBO) potential energy expression for hydrocarbons. *J. Phys-Condens. Mat.* **2002,** *14*, 783.

37. Ni, Y.; Jiang, J.; Meletis, E.; Dumitrică, T., Thermal transport across few-layer boron nitride encased by silica. *Appl. Phys. Lett.* **2015,** *107*, 031603.

38. A. Stukowski, A. Arsenlis, On the elastic–plastic decomposition of crystal deformation at the atomic scale. *Model. Simul. Mater. SR*, **2012**, 20, 035012.

39. M. L. Falk, J. S. Langer, Dynamics of viscoplastic deformation in amorphous solids. *Phys. Rev. E*, **1998**, 57, 7192.

40. J. Liu, X. J., S. Iishi, V. Shalaev, and J. Irudayaraj, Quantifying the local density of optical states of nanorods by fluorescence lifetime imaging. *New J. of Physics*, **2014**, 16, 063069.

Graphical Abstract

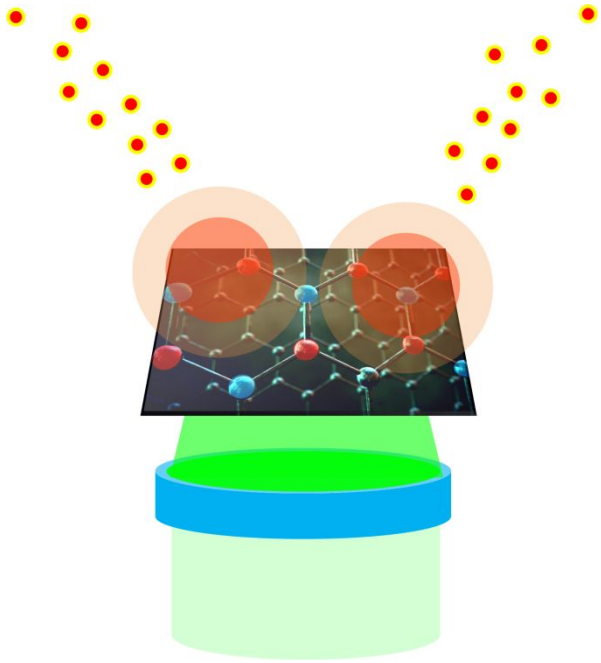

Graphene/BN heterolayered stack act as excellent electronic as well as photonic metamaterials.

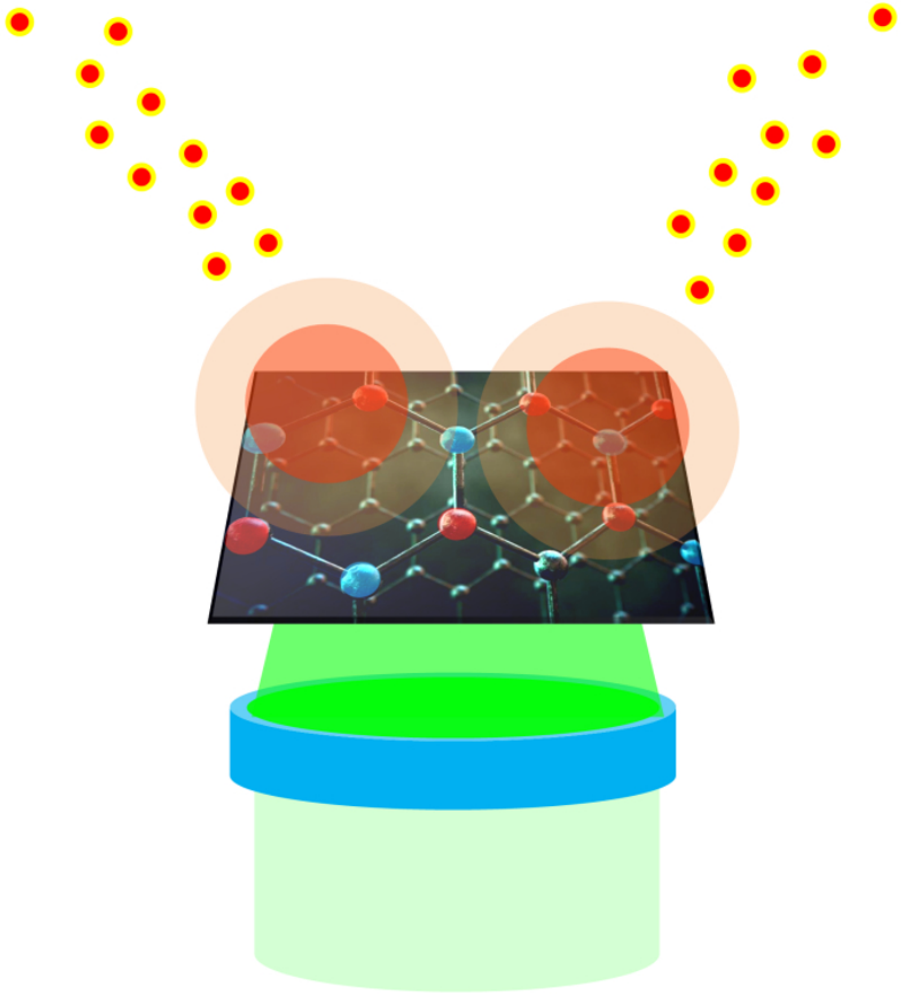

Graphene/BN heterolayered stack act as excellent electronic as well as photonic metamaterials.